

Adatoms-Induced Local Bond Contraction, Quantum Trap Depression, and Charge Polarization at Pt and Rh Surfaces

Chang Q. Sun,^{*,†,‡} Yan Wang,[†] Yanguang Nie,[†] Yi Sun,[§] Jisheng Pan,[§] Likun Pan,^{||} and Zhuo Sun^{||}

School of Electrical and Electronic Engineering, Nanyang Technological University, Singapore 639798, Institute of Materials Research and Engineering, Agency for Science, Technology and Research (A*STAR), Singapore 117602, Engineering Research Center for Nanophotonics & Advanced Instrument, Ministry of Education, Department of Physics, East China Normal University, Shanghai 200062, China, and Faculty of Materials, Optoelectronics and Physical Science and Key Laboratory of Low-Dimensional Materials and Application Technologies (Xiangtan University), Ministry of Education, Changsha 411105, China

Received: August 25, 2009; Revised Manuscript Received: November 18, 2009

The extremely high catalytic efficiency of undercoordinated noble metal adatoms is indeed fascinating, but its chemical and electronic origin remains yet puzzling. Incorporating the BOLS correlation theory [Sun, C. Q. *Prog. Solid State Chem.* **2007**, *35*, 1] into the high-resolution XPS measurements [Baraldi, A.; et al. *New J. Phys.* **2007**, *9*, 143; Bianchettin, L.; et al. *J. Chem. Phys.* **2008**, *128*, 114706] has affirmed the BOLS expectations that the broken bonds induce local strain and quantum trapping in addition to polarization of the otherwise conductive half-filled s-shell charge by the tightly- and densely-trapped inner electrons of the adatoms. Both the trapped and polarized states would be detectable from the density-of-states evolution of the valence and the core bands. The trapped states have been discovered at the bottom edges of Pt($5d^{10}6s^0$) $4f_{7/2}$ and Rh $3d_{5/2}$ bands, and the polarized states only present at the upper edge of Rh($4d^{85}s^1$) $3d_{5/2}$. It is suggested that the quantum trapping increases the electroaffinity and the polarization does oppositely. Therefore, the Rh adatom serves as a donor and the Pt adatom as an acceptor in the process of catalytic reaction.

1. Introduction

Interaction between undercoordinated atoms has been recognized as the key to the unusual behavior of low-dimensional systems such as adatoms, atomic defects, dimers, atomic chains, terrace edges, nanoribbons, nanotubes, nanowires, nanograins, nanocavities, and the skin of a flat surface. The low-dimensional systems are characterized by a high fraction of atoms with an effective atomic coordination number (z , or CN) being between the values of 0 and 12.¹ The z equal to zero corresponds to an isolated atom and $z = 12$ to an atom in the ideal bulk interior with an fcc structure as the standard. The elucidation of the electronic structure and the electronic binding energy (BE) of such low-dimensional systems is of great importance, since its clarification can improve our understanding of the origination of the novel chemical and physical properties of low-dimensional systems, such as the mechanical strength, chemical reactivity, thermal stability, optoelectronic, and magnetic and dielectric performance, as opposed to those of the bulk counterparts.²

The primary role of undercoordinated atoms in determining the surface chemical reactivity has been well-established as a result of surface science. It has been found that³ every third row of Au atoms adding to a fully Au-covered TiO_2 surface could improve the efficiency of CO oxidation at room temperature by a factor of 50 compared with the otherwise fully Au-covered surface. In the case of N_2 dissociation on Ru(0001) surface, the activation energy is 1.5 eV lower at steps than that

on the flat surface, yielding at 500 K a desorption rate that is at least 9 orders of magnitude higher on the terraces, as the dissociation is largely influenced by the presence of steps.⁴ Similar results have been found for NO decomposition on Ru(0001),^{5,6} H_2 dissociation on Si(001),⁷ and low-temperature nitridation of nanopatterned Fe surface.⁸ An adatom concentration of a few percent is sufficient to dominate the overall reaction rate in a catalytic process because of the higher reaction rate or the lower activation energies of the undercoordinated atoms. For instances, the first methane dehydrogenation process is highly favorite at the Rh-adatom site on Rh(111) surface with respect to step or terrace sites,^{9,10} adatoms deposited on oxides can activate the C–H bond scission,¹¹ the acetylene cyclomerization,¹² and the CO oxidation.¹³ Another relevant contribution determining the chemical reactivity is the surface strain. Gsell et al.^{14,15} found preferential oxygen and carbon monoxide adsorption on the stretched regions obtained through subsurface argon implantation on Ru(0001). Wintterlin et al.¹⁶ measured an enhanced NO dissociation probability at the local expanded areas of the Ru(0001) dislocations. In the case of a supported nanoparticle catalyst, it has been observed that adsorption on small clusters can induce a considerable stress in the surface region.¹⁷ In any case, the existence of strain, originated by surface defects or by the interaction with the support, seems to be a general feature of surface catalysts. Obviously, the ability of accepting or donating charge of a catalyst plays a key role in the process of catalytic reaction.¹⁸ The electroaffinity is tunable by the cluster size through valence charge polarization or quantum trapping.¹⁹ The stress is related to the quantum trapping through interatomic binding energy variation.

The extremely high catalytic efficiency of undercoordinated atoms is indeed fascinating. However, the underlying mechanism

* Corresponding author. E-mail: ecqsun@ntu.edu.sg.

[†] Nanyang Technological University.

[‡] Xiangtan University.

[§] Agency for Science, Technology and Research.

^{||} East China Normal University.

has been still a great challenge. The catalytic activity of gold was attributed entirely to the presence of neutral gold adatoms on the gold nanoparticles.³ These adatoms differ from atoms on bulk gold in three ways that might enhance their catalytic activity:³ (i) They have fewer nearest-neighbor atoms and *possibly* a special bonding geometry to other gold atoms that creates a more reactive orbital. (ii) They exhibit quantum size effects that *may* alter the electronic band structure of gold nanoparticles. (iii) They *may* undergo electronic modification by interactions with the underlying oxide that cause partial electron donation to the gold cluster. Therefore, atomic-level understanding of the energetic behavior of electrons of low-dimensional systems is a very important issue in condensed matter science. The understanding of the local energetic behavior of electrons and mechanical properties becomes especially important in systems with a large number of highly undercoordinated atoms.

The objective of this work is to show that incorporating the bond order–length–strength (BOLS) correlation theory^{20,21} into the high-resolution XPS measurements^{22,23} has affirmed the BOLS predictions that the broken bonds induce local strain and charge and energy quantum trapping in addition to polarization of the otherwise conductive half-filled s-shell charge by the tightly- and densely-trapped inner-shell electrons of the adatoms. Both the trapped and polarized states can be identified by monitoring the evolution of the density-of-states in either the valence or the core band because charge polarization takes place in the valence band but the core charge will be screened. In the currently reported work, the adatoms-induced trapping states have been identified at the bottom edges of Pt(5d¹⁰) 4f_{7/2} and Rh(5s¹⁴d⁸)3d_{5/2} band and the polarized states only observable at the upper edge of Rh 3d_{5/2} because of the occupancy of the 5s orbital. From the findings of quantum trapping and polarization, we suggest that Rh adatoms may serve as a donor because of the polarization effect and the Pt as an acceptor due to the quantum-trapping effect, in the process of catalytic reaction.

2. Principle: BOLS Expectations

The BOLS correlation theory² indicates that if one bond breaks, the remaining ones nearby become shorter and stronger. The bonds between the undercoordinated atoms will contract from the bulk value of d_0 to $d_z = C_z d_0$, and the bond energy will increase from the standard bulk value of E_0 to $E_z = C_z^{-m} E_0$. The bond strengthening is represented by the depression of the interatomic potential, which provides the well of quantum trapping. The C_z is the bond contraction coefficient represented by $C_z = 2/\{1 + \exp[(12 - z)/8z]\}$, with z being the effective atomic CN.² The bond nature indicator for metal, m , has been optimized to be around 1. The effective z value for a flat surface atom is 4 instead of 6. The corresponding $C_4 = 0.88$ is inconsistent with many experimental observations. For example, a 12% contraction of the first interatomic Nb(001) layer leads to a 0.50 eV positive shift of the Nb 3d_{3/2} core level;²⁴ a (10 ± 3)% contraction of the first layer spacing has caused the Ta(001) – 4f_{5/2(7/2)} level to shift positively by 0.75 eV.²⁵

As a consequence of the BOLS correlation, localized densification of charge and energy occurs. The broken-bond-induced local strain and quantum trapping provides perturbation to the Hamiltonian Δ_z at the z -coordinated adatom site:

$$\begin{cases} H = \left[-\frac{\hbar^2 \nabla^2}{2m} + v_{\text{atom}}(r) \right] + V_{\text{cry}}(1 + \Delta_z) \\ \Delta_z = C_z^{-m} - 1 \end{cases} \quad (1)$$

The integral of the intraatomic potential, $v_{\text{atom}}(r)$, and the specific Bloch wave function determines the ν th level binding energy of an isolated atom, $E_\nu(0)$; the overlap and exchange integrals of the interatomic potential, $V_{\text{cry}}(1 + \Delta_z)$, with the respective wave functions determine the energy shift from $E_\nu(0)$ to a lower energy upon $V_{\text{cry}}(1 + \Delta_z)$ being involved,²⁶ $\Delta E_\nu(z) = E_\nu(z) - E_\nu(0)$, which is proportional to the equilibrium bond energy, E_z .² Therefore, the broken-bond-induced bond energy gain will directly affect the core-level shift.^{27–29}

The measured XPS spectrum can be decomposed into component Gaussian peaks with each component corresponding to a particular value of z , as illustrated in Figure 1. S₁, S₂, and B are three main peaks. If defects or adatoms present, A₁ and A₂ will appear at the lower (large absolute value) end of the spectrum. The energy values of the components satisfy the following criterion: $\Delta E_\nu(z):\Delta E_\nu(12) = E_z:E_0 = C_z^{-m}$. If polarization occurs, P component presents at the higher end of the spectrum. The energy of the P peak satisfies $\Delta E_\nu(P):\Delta E_\nu(12) = \gamma < 1$, because of the screening effect of the polarization. The γ is the strength ratio of bond energies. The intensities of the components are proportional to the fractions of the specifically z -coordinated atoms. Any core band should demonstrate the fingerprints of both the trapped and the polarized states, if the latter exists. A subtraction of the valence or the core band spectrum of the clean surface from that with adatoms will distinguish the polarized and trapped states.

The broken-bond-induced skin-depth energy densification has been intensively verified for nanostructures because the enhanced energy density relates directly to the local elastic modulus.³⁰ The densely- and tightly-trapped inner-shell charges will polarize existing surface nonbonding electrons such as those in the half-filled s-orbital of metals. The localized polarization of the surface nonbonding s-electrons makes Au, Rh, Ru, and Ag nanocrystals to be nonconductive and magnetic¹⁸ because the otherwise conducting electrons turn to be the tightly-locked monopoles. As a result of the potential trap depression, the gap between the conduction and the valence band of a semiconductor will expand³¹ and the core-level binding energy of a specimen will shift positively to deeper energies, which has been observed frequently.^{2,21,32}

The electroaffinity (in eV) of a specimen is the separation between the vacuum level and the bottom edge of the conduction band, which represents the ability of capturing and holding the bonding electrons from others. One specimen with a larger value of affinity has a higher tendency to hold the caught electrons more firmly; otherwise, the specimen will be ready to lose electrons and serve as a donor. If quantum trapping occurs, the valence charge will flow from the valence top to deeper energies and hence the affinity will be enlarged; the empty states in the upper edge will make the specimen an acceptor that catches electrons from adsorbates. Otherwise, if polarization takes place, the situation changes, and the specimen will provide electrons to the adsorbed specimen in the process of catalytic reaction.

From the perspectives of chemical bonding and the unusual electronic and energetic configurations near the undercoordinated atoms, we have also proposed that the Coulomb repulsion between the “electric monopoles or dipoles locked in the elastic solid skins or the solid-like elastic liquid skins” dominates the occurrences of superhydrophobicity, superfluidity, superlubricity, and supersolidity at the nanometer-sized liquid–solid or

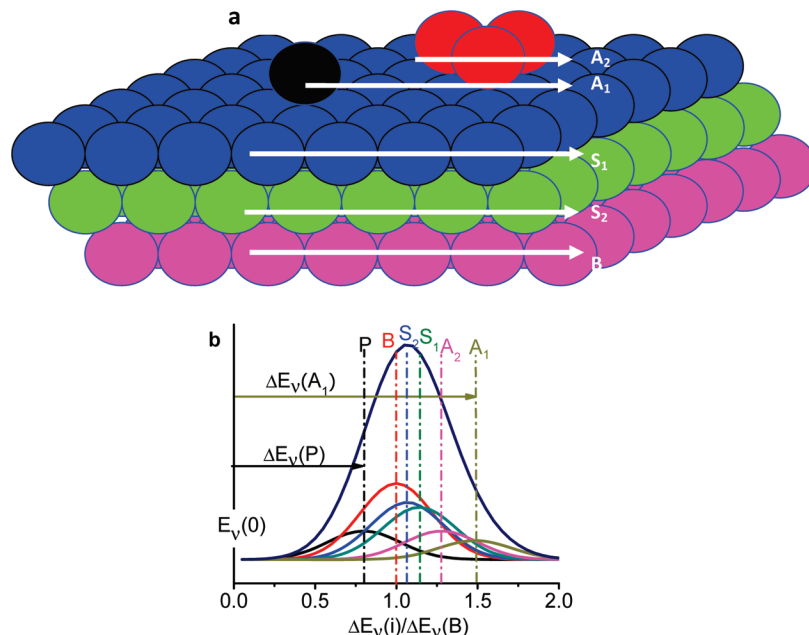


Figure 1. Illustration of the origin for the adatom- and surface-induced core-level shift. (a) Atomic arrangement at a surface with irregularly grown adatoms, A_1 and A_2 with effective CN smaller than 4. S_1 , S_2 , and B represent the outmost, the second, and the bulk components. These XPS components satisfy the following criteria (b): 1. In addition to the main peaks of B, S_2 , S_1 , there should be A and P components representing the trapped and the polarized states of the undercoordinated adatoms. 2. The energy shift should be positive and the lower- z component shifts further. However, the P states should move oppositely with respect to the A states. 3. The energy shift of each component is proportional to the magnitude of bond energy, which follow this relationship: $\Delta E_V(i):\Delta E_V(B) = E_i:E_b = c_i^{-m}$ ($i = A, S_1, S_2$).

solid–solid contacting interfaces.¹ Unfortunately, confirmation of the BOLS expectations of adatom quantum trapping and charge polarization is not so frequent but highly demanding.

From the above discussions, we may establish the rules for decomposing the spectrum of the adatom-induced core-level shift:

1. In addition to the main peaks of B, S_2 , and S_1 , there should be A and P components representing the trapped and the polarized states of the undercoordinated adatoms.

2. The energy shift should be positive, and the lower- z component shifts further. However, the P states should move oppositely to the A states.

3. The energy shift of each component is proportional to the magnitude of bond energy, which follows this relationship: $\Delta E_V(i):\Delta E_V(B) = E_i:E_b = c_i^{-m}$ ($i = A, S_1, S_2$).

3. Results and Discussion

3.1. Experimental Observations: Adatoms Induce Positive Core-Level Shift. The well-measured sets of XPS data from Pt²² and Rh²³ surfaces with adatoms make the current verification of the BOLS expectations possible. Using high-resolution XPS, Baraldi et al.²³ examined the adatom effect up to 1/4 ML on the 3d_{5/2} spectra of Rh(110) and Rh(111) surfaces at photon energy of 380 eV with polar emission angles varying from 20 to 50° with respect to the surface normal. Results showed that the smaller polarization angle from the Rh(111) surface derives a relatively higher intensity of the high-energy bulk component; at the given polar angle and beam energy, the intensity of the low-energy surface peak increases with the coverage of the adatoms compared with other peaks at higher bulk BE of Rh(100). These observations demonstrate the sequence of positive shift. Bianchetti et al.²² also examined the adatom effect up to 0.19 ML on the Pt 4f_{7/2} and decomposed the spectra using two peaks; one is at 71.0 eV and the other around 70.5 eV. The intensity of the 71.0 peak increases with the coverage

of adatom compared to that of the 70.5 eV peak, being consistent with that observed from Rh surfaces.

In order to compare the spectral intensity evolution upon adatoms deposition, we need to find the spectral intensity difference between the spectra collected from specimens with different amount (ML coverage) of adatoms and the spectrum from the ideally clean surface as a standard. Before doing so, we need to normalize all the spectra using the commonly maximum intensity as reference. For Pt 4f_{7/2}, the maximum is at 70.52 eV; for Rh 3d_{5/2}, it is at 307.13 eV. Normalization of all the compared spectra in one set using the highest intensity at certain energy of all the spectra will ensure the full information to be properly analyzed, including the charge polarization and trapping. Figure 2a and b compares the normalized spectra that were collected from Rh and Pt surfaces with different coverage of adatoms. The overlapping of the spectra can hardly show the details clearly regarding the spectral evolution upon homoadsorption of the surfaces.

3.2. Spectral Difference: Presence of Polarized and Trapped States. In order to view closely the spectral difference, we subtracted the normalized spectrum of the clean surface from those with adatoms. The differential spectra are compared in Figure 2c and d. As expected, no polarized features present at all for Pt specimen. However, the Rh profiles are more complicated. In addition to the trapped states at energies of $z = 4$ and 6, the original trapped states at $z = 3$ disappear with an addition of the polarized P states centered at 306.2 eV, above the bulk component. It is seen that the extent of trapping and polarization increases with the adatom coverage up to 0.25 ML. Further deposition may reduce the extent although experimental evidence is lacking from the available database.

The spectral difference between Pt and Rh coincides exceedingly well with the BOLS expectation that only the otherwise conductive half-filled s-electron Rh(4d⁸s¹) can be polarized and locked as monopoles to the adatoms, making no contribution

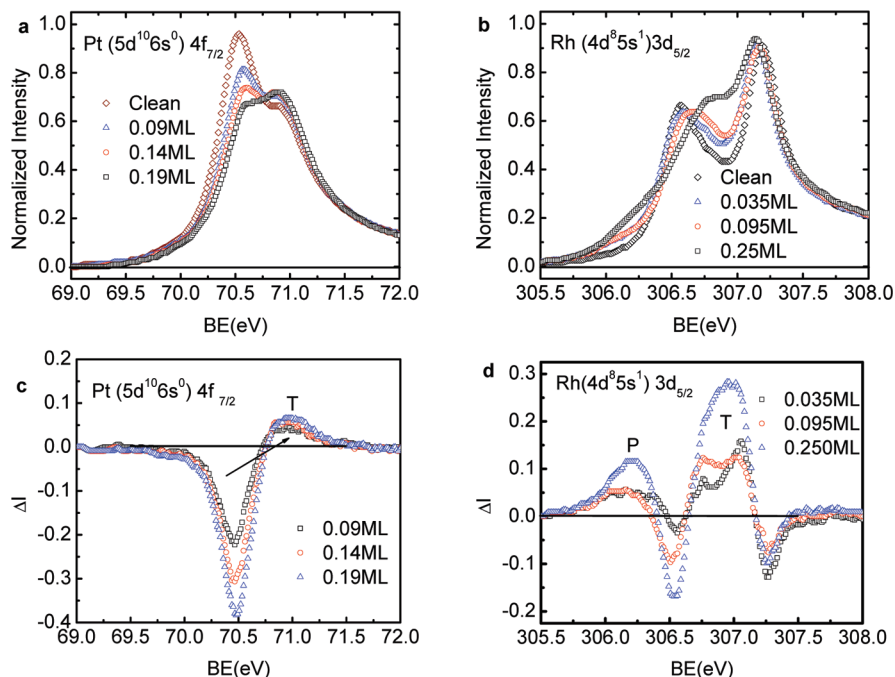


Figure 2. Comparison of the subtracted spectra for surfaces with varied coverage of adatoms by the spectra of clean surfaces of (a) Pt $4f_{7/2}$ ²² and (b) Rh $3d_{5/2}$.²³ Indicated numbers are the effective atomic CNs for bulk (12), surface layers (4, 6), and adatoms (<4). The spectral differences in (c) and (d) show clearly the presence of quantum-trapping effect in both cases and (d) the dominance polarization effect in Rh, which differentiates Pt from Rh adatoms in catalytic reactions.

to the conductivity. These polarized *s*-electrons are suggested to be responsible for the magnetism of the small clusters as well.^{2,33} It has been confirmed that the valence and the core electrons of a specimen shift simultaneously in the same direction because of the screening effect to the core charge, such as the cases of AgPd and CuPd bimetallic alloy catalysts.^{34,35} AgPd was identified as a donor and CuPd as an acceptor because of the respective polarization and trapping effect.

There are two possible reasons for the loss of the initially trapped surface charge at $z = 3$: (i) the electrons of adatoms are fully polarized, moving from $z = 3$ energy to the P states; (ii) the number of the initially $z = 3$ adatoms is reduced upon deposition of adatoms, which means that the initial flat surface is not so flat but with many edges and steps. Compared with the XPS Pd $3d_{5/2}$ profiles, the XPS $3d_{5/2}$ spectra of Rh surfaces demonstrate asymmetric features.^{23,36} The tails at the lower energy end indicate the presence of surface defects trapped states. From the analysis, it is understandable now why there is no such P states in the Pt($5d^{10}6s^0$) $4f_{7/2}$ spectra because of the unoccupied 6s orbit.

Similarly, we have examined the residual Pt $4f_{7/2}$ DOS of Pt(100)–(1×1)³⁷ induced by the hexagonally reconstructed Pt(100) surface, as shown in Figure 3. The simple subtraction of the spectrum of the hexagonally reconstructed surface with denser edges by that of the perfect Pt(100)–(1×1) surface revealed that the residual density of state follows the trend in Figure 2c of quantum trapping. Due to a contraction of the Pt–Pt distance, the topmost layer accommodates about 25% more atoms than the bulk-terminated ideal (100) layer. This finding further supports the BOLS derivatives regarding the structural relaxation and quantum trap depression by the shorter and stronger bonds between undercoordinated atoms.

3.3. Decomposition: Quantification of the Energy Levels and Their Components Shift. According to the constraints given, the spectra from clean surface of each Pt and Rh specimen

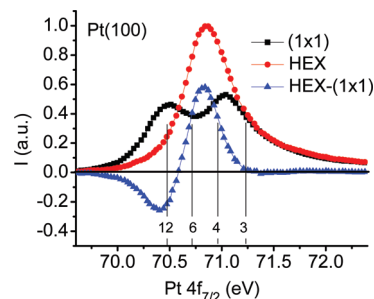


Figure 3. XPS data for Pt(100)–(1×1) and the hexagonally reconstructed Pt(001) surface with denser edges. The residual DOS exhibits the bulk valley and the general trend of quantum trapping caused by the shorter and stronger bonds between undercoordinated atoms. The residual is scaled with indication of the effective atomic coordination numbers of 12, 6, 4, and 3.

were decomposed with five components, representing the P, B, S₂, S₁, and A from higher to lower BE, as shown in Figure 4. The decomposition was conducted by choosing $z_1 = 4$ and $z_3 = 12$ for the (100) surface as reference and allowing other components to be optimized in the best fit. For each element, the B energy and $E_v(0)$ remain unchanged for all the surfaces. The optimal component energies and the decomposition parameters are summarized in Table 1. The derived local strain ($c_z - 1$) and the effective CNs for the other components are also given.

From the decomposition, we obtained the $E_v(0)$ and $\Delta E_v(i)$ values. Using a least root-mean-square method,²¹ we can obtain the standard deviation. It has been derived that the BE for an isolated Rh atom is 302.1467 ± 0.0003 eV with the bulk shift of 4.3653 eV and that the BE for an isolated Pt atom is 67.2086 ± 0.0003 eV with the bulk shift of 3.2814 eV. The refinement leads to the effective atomic CNs of the top (100) and (111) atomic layers as 4.00 and 4.25.

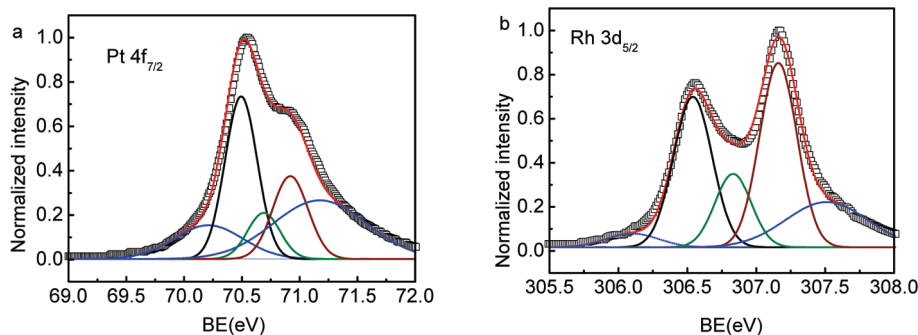


Figure 4. Decomposed XPS spectra of the (a) Pt(111) and (b) Rh(100) clean surfaces with five components each representing the polarized P, bulk B, surfaces S_1 and S_2 , and the adatom A states from lower (larger absolute value) to higher BE. The decomposition parameters are listed in Table 1.

TABLE 1: Summary of Decomposition Parameters (BE, Binding Energy; W , Width; I , Intensity) for the Pt and Rh Spectra and the BOLS Derived Effective CN(z), Local Strain ($c_z - 1$), Ratio of Binding Energy Density (c_z^{-4}), and Ratio of Atomic Cohesive Energy ($z/z_b c_i^{-1}$) for Each Surface and Adatom Component^a

		P	B	S_2	S_1	A
Pt(111) $4f_{7/2}$	BE	70.21	70.49	70.69	70.91	71.18
	W	0.70	0.33	0.33	0.36	0.95
	I	0.15	0.73	0.21	0.37	0.26
	z	—	12	6.25	4.25	3.15
	$c_z - 1$	—	0	-0.05	-0.113	-0.174
	c_z^{-4}	—	1	1.27	1.62	2.15
	$z/z_b c_i^{-1}$	—	1	0.55	0.40	0.32
Rh(100) $3d_{5/2}$	BE	306.10	306.53	306.85	307.15	307.51
	W	0.45	0.33	0.31	0.32	0.70
	I	0.09	0.70	0.34	0.85	0.22
	z	—	12	5.73	4.0	3.0
	$c_z - 1$	—	0	-0.068	-0.124	-0.183
	c_z^{-4}	—	1	1.327	1.700	2.248
	$z/z_b c_i^{-1}$	—	1	0.5129	0.381	0.308

^a $z_b = 12$. $E_v(0)$ is the energy level of an isolated atom. The coordination resolved component BE follows eq 2.

The calculations lead to the coordination-resolved core-level shift for Rh $3d_{5/2}$ and Pt $4f_{7/2}$

$$E_v(z) = \langle E_v(0) \rangle \pm \sigma + \Delta E_v(B) c_z^{-1} \\ = \begin{cases} 302.1647 \pm 0.0003 + 4.3653 c_z^{-1} & (\text{Rh}3d_{5/2}) \\ 67.2086 \pm 0.0003 + 3.2814 c_z^{-1} & (\text{Pt}4f_{7/2}) \end{cases} \quad (2)$$

with an addition of the polarized states to the Rh adatoms. Theoretical reproduction of the size dependence of the Pt $3d_{5/2}$ spectra has led to the bulk shift of 2.99 ± 0.31 eV and the $E_{3d}(0) = 67.67$ eV. The difference may arise from the accuracy of particle size determination. This fundamental information should be useful to the understanding of the catalytic behavior of these undercoordinated atoms.

Besides the effective atomic CN and the local strain ($c_z - 1$), decomposition of the XPS spectra allows us to derive information regarding the ratio of binding energy density (c_z^{-4}), and the ratio of atomic cohesive energy ($z/z_b c_i^{-1}$) for each surface and adatom component,² as listed in Table 1. These quantities are of fundamental importance to the understanding of the surface properties and the processes of surface reaction and nucleation. For instance, the binding energy density determines uniquely the elastic modulus³⁰ and the atomic cohesive energy dominates the critical temperature of phase transition.¹

4. Conclusion

We have analyzed the homoatom XPS spectra of Pt $4f_{7/2}$ and Rh $3d_{5/2}$ based on the recently developed BOLS theory and

algorithm with derived quantitative information and improved understanding of the catalytic behavior of the undercoordinated atoms:

1. The expectations of broken-bond-induced local strain and quantum trapping and the associated polarization of nonbonding electrons have been confirmed.

2. The spectral difference provides a powerful tool for identifying the evolution of electrons upon coordination change.

3. The five-component spectral decomposition allows us to extract quantitative information about the energy levels of an isolated atom and to establish the coordination-resolved BE of each component and the corresponding local lattice strain.

4. Approaches and findings may extend to other undercoordinated systems such as atomic defects and nanostructures.

5. Most importantly, the Rh adatom has been identified as a donor and Pt adatom as an acceptor in the catalytic reactions because of the XPS-detected respective polarization and quantum-trapping effect.

6. Besides the effective atomic CN and the local strain, decomposition of the XPS spectra allows us to derive information regarding the ratio of binding energy density and the ratio of atomic cohesive energy for each surface and adatom component, which are of fundamental importance to the understanding of the surface properties and the processes of surface reaction and nucleation.

Acknowledgment. Financial support from Nanyang Technological University and Agency for Science, Technology and Research, Singapore, Nature Science Foundation (No.10772157)

of China, Shanghai Natural Science Foundation (No. 07ZR14033), Shanghai Pujiang Program (No. 08PJ14043), Special Project for Nanotechnology of Shanghai (No. 0752 nm011), and Applied Materials Shanghai Research & Development Fund (No. 07SA12) are all gratefully acknowledged.

References and Notes

- (1) Sun, C. Q. *Prog. Mater. Sci.* **2009**, *54*, 179.
- (2) Sun, C. Q. *Prog. Solid State Chem.* **2007**, *35*, 1.
- (3) Chen, M. S.; Goodman, D. W. *Science* **2004**, *306*, 252.
- (4) Dahl, S.; Logadottir, A.; Egeberg, R. C.; Larsen, J. H.; Chorkendorff, I.; Tornqvist, E.; Norskov, J. K. *Phys. Rev. Lett.* **1999**, *83*, 1814.
- (5) Hammer, B. *Phys. Rev. Lett.* **1999**, *83*, 3681.
- (6) Zambelli, T.; Wintterlin, J.; Trost, J.; Ertl, G. *Science* **1996**, *273*, 1688.
- (7) Kratzer, P.; Pehlke, E.; Scheffler, M.; Raschke, M. B.; Hofer, U. *Phys. Rev. Lett.* **1998**, *81*, 5596.
- (8) Tong, W. P.; Tao, N. R.; Wang, Z. B.; Lu, J.; Lu, K. *Science* **2003**, *299*, 686.
- (9) Fratesi, G.; de Gironcoli, S. *J. Chem. Phys.* **2006**, *125*, 044701.
- (10) Kokalj, A.; Bonini, N.; Sbraccia, C.; de Gironcoli, S.; Baroni, S. *J. Am. Chem. Soc.* **2004**, *126*, 16732.
- (11) Abbet, S.; Sanchez, A.; Heiz, U.; Schneider, W. D.; Ferrari, A. M.; Pacchioni, G.; Rosch, N. *J. Am. Chem. Soc.* **2000**, *122*, 3453.
- (12) Abbet, S.; Heiz, U.; Hakinen, H.; Landman, U. *Phys. Rev. Lett.* **2001**, *86*, 5950.
- (13) Zhang, C. J.; Hu, P. *J. Chem. Phys.* **2002**, *116*, 4281.
- (14) Jakob, P.; Gsell, M.; Menzel, D. *J. Chem. Phys.* **2001**, *114*, 10075.
- (15) Gsell, M.; Jakob, P.; Menzel, D. *Science* **1998**, *280*, 717.
- (16) Wintterlin, J.; Zambelli, T.; Trost, J.; Greeley, J.; Mavrikakis, M. *Angew. Chem., Int. Ed.* **2003**, *42*, 2850.
- (17) Richter, B.; Kuhlbeck, H.; Freund, H. J.; Bagus, P. S. *Phys. Rev. Lett.* **2004**, *93*, 026805.
- (18) Roduner, E. *Chem. Soc. Rev.* **2006**, *35*, 583.
- (19) Sun, C. Q.; Shi, Y.; Li, C. M.; Li, S.; Yeung, T. C. A. *Phys. Rev. B* **2006**, *73*, 075408.
- (20) Sun, Y.; Wang, Y.; Pan, J. S.; Wang, L. L.; Sun, C. Q. *J. Chem. Phys. C* **2009**, *113*, 14696.
- (21) Sun, C. Q. *Phys. Rev. B* **2004**, *69*, 045105.
- (22) Bianchettin, L.; Baraldi, A.; de Gironcoli, S.; Vesselli, E.; Lizzit, S.; Petaccia, L.; Comelli, G.; Rosei, R. *J. Chem. Phys.* **2008**, *128*, 114706.
- (23) Baraldi, A.; Bianchettin, L.; Vesselli, E.; de Gironcoli, S.; Lizzit, S.; Petaccia, L.; Zampieri, G.; Comelli, G.; Rosei, R. N. *J. Phys. (Paris)* **2007**, *9*, 143, 12.
- (24) Fang, B. S.; Lo, W. S.; Chien, T. S.; Leung, T. C.; Lue, C. Y.; Chan, C. T.; Ho, K. M. *Phys. Rev. B* **1994**, *50*, 11093.
- (25) Bartynski, R. A.; Heskett, D.; Garrison, K.; Watson, G.; Zehner, D. M.; Mei, W. N.; Tong, S. Y.; Pan, X. *J. Vac. Sci. Technol., A* **1989**, *7*, 1931.
- (26) Omar, M. A. *Elementary Solid State Physics: Principles and Applications*; Addison-Wesley: New York, 1993.
- (27) Aruna, I.; Mehta, B. R.; Malhotra, L. K.; Shivaprasad, S. M. *J. Appl. Phys.* **2008**, *104*, 064308.
- (28) Balamurugan, B.; Maruyama, T. *Appl. Phys. Lett.* **2006**, *89*, 033112.
- (29) Suprun, S. P.; Fedosenko, E. V. *Semiconductors* **2007**, *41*, 590.
- (30) Liu, X. J.; Li, J. W.; Zhou, Z. F.; Yang, L. W.; Ma, Z. S.; Xie, G. F.; Pan, Y.; Sun, C. Q. *Appl. Phys. Lett.* **2009**, *94*, 131902.
- (31) Ma, D. D. D.; Lee, C. S.; Au, F. C. K.; Tong, S. Y.; Lee, S. T. *Science* **2003**, *299*, 1874.
- (32) Matsui, F.; Matsushita, T.; Kato, Y.; Hashimoto, M.; Inaji, K.; Guo, F. Z.; Daimon, H. *Phys. Rev. Lett.* **2008**, *100*, 207201.
- (33) Cox, A. J.; Loudnerback, J. G.; Apsel, S. E.; Bloomfield, L. A. *Phys. Rev. B* **1994**, *49*, 12295.
- (34) Sun, C. Q. Communicated 2009.
- (35) Khanuja, M.; Mehta, B. R.; Shivaprasad, S. M. *Thin Solid Films* **2008**, *516*, 5435.
- (36) Andersen, J. N.; Hennig, D.; Lundgren, E.; Methfessel, M.; Nyholm, R.; Scheffler, M. *Phys. Rev. B* **1994**, *50*, 17525.
- (37) Baraldi, A.; Vesselli, E.; Bianchettin, L.; Comelli, G.; Lizzit, S.; Petaccia, L.; de Gironcoli, S.; Locatelli, A.; Menten, T. O.; Aballe, L.; Weissenrieder, J.; Andersen, J. N. *J. Chem. Phys.* **2007**, *127*, 164702.

JP908220A